Main Manuscript for

Cataract-prone variants of γD-crystallin populate a conformation with a partially unfolded N-terminal domain under native conditions

Sara Volz[1,2], Jadyn R. Malone[3,4], Alex J. Guseman[5], Angela M. Gronenborn[5] and Susan Marqusee[2,6,7*]

1. Biophysics Graduate Program, University of California, Berkeley, Berkeley CA 94305
2. California Institute for Quantitative Biosciences – QB3 Berkeley
3. Department of Chemistry and Biochemistry, College of Letters and Science, Montana State University, Bozeman, MT 59717
4. Department of Microbiology and Cell Biology, College of Agriculture, Montana State University, Bozeman, MT 59717
5. Department of Structural Biology, University of Pittsburgh School of Medicine, Pittsburgh, Pennsylvania 15213
6. Department of Molecular and Cell Biology, University of California, Berkeley, Berkeley CA 94305
7. Department of Chemistry, University of California, Berkeley, Berkeley CA 94305

*Corresponding author: Susan Marqusee

Email: marqusee@berkeley.edu

Author Contributions: S.V., A.J.G, A.M.G, and S.M. designed research; S.V carried out experimental studies with assistance from J.R.M.; S.V. and S.M. analyzed data; S.V., A.J.G, A.M.G, and S.M. wrote and edited the manuscript.

Competing Interest Statement: The authors declare no competing interests.

Classification: Major: Biological Sciences, Minor: Biophysics and Computational Biology.

Keywords: γD-crystallin, cataract formation, protein folding, aggregation

This PDF file includes:

Main Text
Figures 1 to 6
Tables 1 to 2

Abstract

Human γD-crystallin, a monomeric protein abundant in the eye lens nucleus, must remain stably folded for an individual's entire lifetime to avoid aggregation and protein deposition-associated cataract formation. γD-crystallin contains two homologous domains, an N-terminal domain (NTD) and a C-terminal domain (CTD), which interact via a hydrophobic interface. Several familial mutations in the gamma crystallin gene are linked to congenital early-onset cataract, most of which affect the NTD. Some of these, including V75D and W42R, are known to populate intermediates under partially denaturing conditions possessing a natively folded CTD and a completely unfolded NTD. We employed hydrogen-deuterium exchange mass spectrometry (HDX-MS) to probe the structural and energetic features of variants of γD-crystallin under both native and partially denaturing conditions. For V75D and W42R, we identify a species under native conditions that retains partial structure in the NTD and is structurally and energetically distinct from the intermediate populated under partially denaturing conditions. Residues at the NTD-CTD interface play crucial roles in stabilizing this intermediate, and disruption of interface contacts either by amino acid substitution or partial denaturation permits direct observation of two intermediates simultaneously. These data suggest that the intermediate identified under native conditions is accessed from the native state and not on the folding pathway. The newly identified intermediate exposes hydrophobic amino acids that are buried in both the folded full-length protein and in the protein's stable isolated domains. Such non-native exposure of a hydrophobic patch may play an important role in cataract formation. (244 words)

Significance Statement

Human γD-crystallin, which plays a structural role in the eye lens, is a long-lived protein that must remain folded for an individual's entire lifetime to avoid aggregation and protein deposition - associated cataract formation. By using hydrogen-deuterium exchange mass spectrometry, we demonstrate that two cataract-associated variants of γD-crystallin populate an intermediate under native conditions with partial structure along the interface between its two domains. In these intermediates, hydrophobic amino acids that are normally buried in the N-terminal domain's native folded structure become exposed, possibly leading to aggregation and cataract formation. Our findings illustrate the importance of studying a protein's energy landscapes under conditions that are close to physiological.

Main Text

Introduction

The lens of the eye is a unique and highly specialized organ subject to specific biophysical constraints. It must be transparent to prevent light scattering or absorption, it must possess a high refractive index to tightly focus light onto the retina, and its focal length must be adjustable to permit focusing over a range of distances (1, 2). To achieve these optical properties, 90% of the protein mass in fully differentiated lens fiber cells consists of soluble, densely packed crystallin proteins at concentrations exceeding 400 mg/ml (3). During lens maturation, all cellular structures that contribute to light scattering are eliminated, including nuclei and organelles, effectively stopping protein turnover in the mature lens (4, 5). Therefore, to maintain faithful functioning of the eye lens, crystallins must remain soluble and stably folded for an individual's entire lifetime. Alas, over years, crystallins are exposed to environmental and chemical assaults, resulting in damage that can initiate aggregation and precipitation. Subsequent opacification of the lens, as seen in age-related cataract, is a condition that affects more than 20 million people and is the leading cause of blindness worldwide (6).

Crystallins are subdivided into three families: α-, β-, and γ-crystallins. α-crystallins are small heat shock proteins that assemble into oligomeric structures, perform holdase chaperone functions,

and assist in homeostasis of β- and γ-crystallins by inhibiting unfolding (7, 8). β- and γ-crystallins, which exist as dimers/oligomers and monomers, respectively, are small, stable proteins with high solubility that play structural roles in conferring the optical properties of the eye lens (9). Human γD-crystallin (γDC) is the second-most abundant γ-crystallin found in the lens nucleus, comprising ~11% by mass of the total protein in young human lenses (10). γDC is relatively small (~21 kDa) with two homologous β-sheet domains, an N-terminal domain (NTD) and a C-terminal domain (CTD), each comprised of two Greek key motifs; the CTD and NTD are connected by a short linker and interact via a nonpolar interface (Figure 1A) (11, 12).

Despite its high thermodynamic and kinetic stability, protein damage to γDC, by UV (13), deamidation (14), oxidation (15), or other modifications, has been proposed to result in aggregation and cataract (16). Furthermore, mutations in the γD-crystallin gene have been linked to early-onset or congenital cataract, including R14C (17), P23T (12, 18), W42R (19) , R58H (20), G60C (21), V75D (22), R76S (23), and I81M (24). Interestingly, for most amino acid changes, including V75D (25) and W42R (26), no significant structural changes are observed, suggesting that differences in folding/unfolding behavior (that is, in the energy landscape) are likely the source of the aggregation-prone behavior.

Upon chemical denaturation, wild-type γDC populates a stable intermediate best characterized as a fully unfolded NTD and a fully folded CTD (27–31). Isolated N-terminal and C-terminal domain fragments of γDC (hereafter termed γDC_{NTD} and γDC_{CTD}) are stable and well-folded. γDC_{NTD} is less stable than γDC_{CTD} despite the fact that they show nearly overlapping unfolding transitions in the context of the full-length protein (28, 32). Therefore, the presence of the CTD stabilizes the NTD in the full-length protein, most likely due to residues in the NTD (C41, M43, F56, R79, I81, and P82) that face the opposing CTD surface (comprising residues V132, G141, Q143, L145, R167, and V169) (12). Past work has estimated this interface contributes 4 kcal/mol (32), and destabilization of these predominantly hydrophobic interactions, as in the CTD variant V132A, results in destabilization of the NTD unfolding transition (31).

Direct characterization of this intermediate has been carried out in the NTD-destabilized variant V75D using both NMR and SAXS. The intermediate, as expected, is comprised of a fully unfolded NTD and a fully folded CTD (25, 33). Destabilization of the NTD in the W42R variant also permits observation of a minor species with NTD unfolding under native conditions (26). It has been proposed that small populations of partially unfolded conformers that are difficult to detect in solution may serve as the nucleus for aggregation, overwhelming the chaperone system and potentially resulting in cataract (26, 33, 34), thus raising the tantalizing possibility that this partially unfolded intermediate might serve as a nucleus for aggregation and/or cataract formation. However, the fact that the individual domains fold and refold in isolation without obvious aggregation is hard to reconcile with this.

Partially structured states accessible under non-native conditions such as those described above may not be identical to the conformations accessed under physiological or native conditions. We therefore used hydrogen–deuterium exchange coupled with mass spectrometry (HDX-MS) to investigate the structural and energetic characteristics of γDC's energy landscape under native and denaturing conditions. While most standard techniques for probing protein stability, such as circular dichroism or fluorescence, are unable to detect minor conformations, HDX-MS has the unique capability to both identify and structurally characterize such rare states.

HDX-MS monitors the exchange of labile hydrogens with solvent deuterons (35). For backbone amides, this exchange requires accessibility to the deuterated solvent and/or transient hydrogen-bond opening. Therefore, fast HDX rates correlate to exposed and flexible regions in the protein, while slow rates are associated with amide hydrogens that are buried within the protein and/or involved in stable hydrogen bonds. The observed rate of exchange can be analyzed using the Linderstrøm-Lang model (36) to determine either the energetics or kinetics for the opening event that exposes the amide (37). HDX-MS is therefore an ideal tool to characterize systems like γDC,

a protein for which potential sub-global unfolding events are particularly germane to function and misfunction.

We found that, for two cataract-associated variants of γDC with destabilizing amino acid changes in the NTD, the partially unfolded state detected under native conditions is not the intermediate populated under denaturing conditions, but rather a distinct species with both a folded CTD and residual structure at the NTD/CTD interface. Our data suggest that this newly identified intermediate exposes a surface that normally is buried, both in the full-length structure and in the isolated folded NTD. Therefore, this intermediate, which does not reside along the folding pathway, is uniquely accessed from the folded state and may represent the pivotal conformer that initiates the aggregation pathway, ultimately resulting in cataract formation.

Results

Equilibrium unfolding/refolding of wild-type and variant proteins

We first used standard GdmCl-induced denaturation to determine the energetics and relative stabilities of the NTD, the CTD, and the NTD-CTD interface of γDC and several variants. Although variants of γDC have already been characterized by chemically induced denaturation, so far all stability data have been analyzed by standard two- or three-state equilibrium unfolding models, using linear extrapolations to zero denaturant (25–28, 31, 38). In order to calculate interfacial interaction energies precisely, and, more importantly, in a consistent manner, we repeated several γDC unfolding studies. We collected equilibrium unfolding curves for the full-length protein and isolated single-domains for several variants.

GdmCl-induced denaturation was monitored by tryptophan fluorescence (Figure 1). γDC contains four tryptophan residues, two in the N-terminal domain (residues 42 and 68) and two in the C-terminal domain (residues 130 and 165). Since all four tryptophans are buried in the native structure and their fluorescence is quenched when γDC occupies the native state, intrinsic tryptophan fluorescence serves as an excellent reporter of unfolding in γDC (39, 40). We examined wild-type γDC, V132A γDC, V75D γDC, V75D/V132A γDC, γDC with five amino acid changes in the CTD that reside in the NTD-facing side of the CTD (V132A/Q143A/L145A/M147A/V169A) (dInt-γDC), the isolated NTD (γDC_{NTD}, residues 1-81), the isolated CTD (γDC_{CTD}, residues 84-174), and the isolated CTD with V132A (V132A-γDC_{CTD}) (Table 1). Data were first analyzed via a two-state ($N \rightleftharpoons U$) or a three-state ($N \rightleftharpoons I \rightleftharpoons U$) linear-extrapolation model, resulting in parameters describing ΔG in the absence of denaturant and the dependence of ΔG upon denaturant (*m*-value) (41, 42). The data for V132A and wild type were subsequently analyzed using a 1D-Ising model (see below) (43, 44).

All isolated domains studied (γDC_{NTD}, γDC_{CTD}, and V132A-γDC_{CTD}) exhibit apparent cooperative two-state behavior, consistent with previously reported equilibrium data (28, 32) and were analyzed using the two-state ($N \rightleftharpoons U$) model (Figure 1B, Table 1). All full-length crystallin constructs studied, except for wild-type γDC, show two transitions with a clear plateau, indicating the presence of an intermediate, and were fit to a three-state model ($N \rightleftharpoons I \rightleftharpoons U$) (Figure 1B). While wild-type γDC has been previously observed to fit well to a three-state model (28, 32), under the conditions used here, the two transitions cannot be distinguished from one another, precluding a three-state fit. The resulting two-state fit, however, yields an unusually broad transition when compared to the isolated domains and is therefore considered to be unreliable, emphasizing the usefulness of an Ising model in dissecting the energetics of each transition (see below).

All full-length variants studied show a destabilization of the first unfolding transition, whether the amino acid changes reside in the NTD or the CTD. Although residue 132 is in the CTD, V132A

mostly impacts the first (NTD-unfolding) transition, suggesting that removing a hydrophobic contact in the region of the CTD that faces the NTD decreases the stability of the NTD in the context of full-length γDC. These data are in agreement with similar studies, albeit collected under different conditions (e.g., temperature) (31).

We used an Ising model to compute the ΔG of each domain and the interfacial ΔG upon association of the two domains. This approach requires measurements for the equilibrium unfolding transitions of both a full-length protein and its individual domains, and it has been successfully applied to repeat proteins that interact via a defined interface (44, 45). We used a global fitting approach for a one-dimensional Ising model comprising a two-repeat heteropolymer as outlined previously (46) to analyze the folding transitions for the full-length γDC variants for which both isolated domain transitions were measured (wild type and V132A) (Figure 1C). Our results are summarized in Figure 1D.

Wild-type γDC data fit well to this 1D-Ising model (reduced sum of squared residuals (RSSR) = 4.11×10^{-4}), with intrinsic folding free energies of -4.5 and -8.2 kcal/mol for the NTD and CTD, respectively, in good agreement with those extracted from the equilibrium unfolding curves of isolated domains. This Ising model also permits us to calculate the an interfacial energy of -3.8 kcal/mol in wild-type γDC, consistent with a previous estimate (32) (Table 1). We therefore conclude that the two domains are strongly energetically coupled.

For V132A, however, the equilibrium unfolding transition is not well-fit by the standard 1D-Ising model, as evidenced by a non-random distribution of fit residuals (RSSR = 1.1×10^{-3}, Figure S1). The second unfolding transition (corresponding to unfolding of the CTD) is stabilized in the full-length V132A protein compared to the isolated domain (V132A-γDC$_{CTD}$), even at concentrations of denaturant where the NTD is fully unfolded. Hence, we hypothesize that in this variant, the presence of the unfolded NTD stabilizes the folded CTD. This is an interaction that is not captured by the simplest version of the 1D-Ising model. Use of an interaction term for describing the stabilization of the folded CTD by the NTD whether the NTD is folded or unfolded (44) yields a significantly improved fit (RSSR = 5.12×10^{-4}, Figure 1C) with an interfacial energy of -1.1 kcal/mol. This represents a reduction in interfacial stability of 2.6 kcal/mol compared to wild type. (An alternative, more complicated version of this model in which the stabilization of the CTD upon interaction with the unfolded NTD was used as a parameter distinct from the stabilization by the folded NTD, i.e. a model that uses two separate interaction terms, did not pass an F-test and was deemed not suitable ($p = 0.49$)). Thus, surprisingly, our analysis of V132A γDC shows that some interfacial stabilization can be conferred by the unfolded NTD. Thus, specific contacts between the two folded domains are lost upon removal of the hydrophobic sidechain of V132.However, stabilizing interfacial interactions in V132A are also mediated via the unfolded NTD, which is not the case for wild type: applying a folded-unfolded interaction term to wild type yields an interaction energy of ~0 kcal/mol, suggesting that loss of specific contacts made by the valine side chain disrupts the interface (Table S1).

In an attempt to completely destabilize the interface, we added more CTD changes at interfacial residues, creating dInt-γDC ((V132A/Q143A/L145A/M147A/V169A). These additional changes destabilize the second unfolding transition by 2.5 kcal/mol, but do not further disrupt the first unfolding transition compared to V132A (Figure S2A). Thus, these further changes to the CTD surface do not destabilize the NTD transition and instead only reduce the intrinsic stability of the CTD.

For technical reasons, we were unable to carry out a full Ising analysis for the V75D variant. The isolated V75D NTD (V75D-γDC$_{NTD}$) proved refractory to purification and analysis, despite multiple attempts. Based on the above data, we predict that V75D-γDC$_{NTD}$ is intrinsically unstable and that most of its stability in the full-length protein is provided by interfacial interactions. The low stability of the first transition of the V75D/V132A variant (in which stabilizing interactions with the CTD are reduced) also points to the intrinsic instability of V75D-γDC$_{NTD}$.

In sum, our Ising analysis quantifies the stability of each individual domain of γDC separately from its interfacial energy, demonstrating that the interface is a significant contributor to the stability of the NTD in the context of the full-length protein, and that V132A reduces both the strength and specificity of the interface.

Continuous-labeling HDX-MS on variants of γD-crystallin

While the above equilibrium experiments and Ising analyses allow a quantitative determination of the stability of each domain and the interfacial coupling between them, they do not inform about the conformations associated with any partially unfolded states. Therefore, we assessed the conformational ensembles of the γDC variants on a sub-global level using HDX-MS. We followed continuous hydrogen-deuterium exchange of wild type and several variants over a time course spanning from 15 seconds to 72 hours, both in the presence and absence of denaturant (PBS pH 7.0, 5 mM DTT, 25 ˚C). The 0 M denaturant conditions are both experimentally tractable and serve as a reasonable surrogate for conditions in the eye lens, including neutral pH (47). The experiments were carried out at 25 ˚C (instead of 37°C), where HDX-MS is technically less challenging; this small temperature difference should not dramatically impact populations of any rare structures observed (48).

The kinetics of HDX are commonly analyzed using two kinetic regimes, EX1 and EX2, which respectively report on either the kinetics or thermodynamics of the fluctuations resulting in exchange. When monitored by mass spectrometry, these two kinetic limits can be distinguished by their mass spectral signatures: EX1 kinetics produce two distinct mass envelopes whose relative intensities change over time without a shift in m/z, while EX2 kinetics result in the gradual increase in m/z over time of a unimodal mass envelope (49). For both regimes, the exchange process can be analyzed via the Linderstrøm-Lang model of HDX (36), where an amide hydrogen interconverts with rates k_{op} and k_{cl} between a closed, exchange-resistant state and an open, exchange-competent state:

$$\text{closed} \underset{k_{cl}}{\overset{k_{op}}{\rightleftharpoons}} \text{open} \xrightarrow{k_{int}} \text{exchanged}$$

In this model, exchange in the open state occurs at a rate k_{int}, the known chemical or intrinsic rate of exchange for a given amide hydrogen. When the rate of closing k_{cl} is slow relative to the intrinsic rate of exchange k_{int} ($k_{cl} << k_{int}$), EX1 applies, and the observed exchange rate is equal to the rate of structural opening k_{op}. Conversely, in the EX2 kinetic exchange limit, the rate of closing k_{cl} is fast relative to the intrinsic rate of exchange k_{int} ($k_{cl} >> k_{int}$). In this regime, the observed rate of hydrogen exchange is related to the free energy of the transition between the high-energy (open) and low-energy (closed) state; specifically, the observed rate constant of exchange can be expressed as $k_{obs} = (k_{op}/k_{cl}) * k_{int} = K_{op} * k_{int}$, with K_{op} the equilibrium constant for opening to the exchange-competent state. Thus, the free energy for opening is $\Delta G_{op} = -RT \ln(k_{obs}/k_{int})$. When exchange is monitored at the peptide level by mass spectrometry, the average intrinsic rate constant k_{int} for that peptide can be estimated based on the sequence of the individual peptide (50). Thus, a given $\Delta G_{unfolding}$ (opening) is associated with an expected HDX rate per peptide. Amide hydrogens in dynamic or flexible regions will exchange more quickly than estimated based on unfolding. However, if the observed EX2 exchange is significantly slower than estimated, an opening event with a ΔG greater than the postulated structural transition must be present.

Using aspergillopepsin and pepsin digestion of the proteins and a two-step quenching method (see Methods), we obtained peptides covering between 95-100% of the sequence for all variants studied. This permitted interrogation of dynamics across all of γDC (average redundancy, coverage, and back exchange as well as other experimental parameters for all variants may be found in Table S2). In most variants, nearly all peptides exhibit a single mass-envelope distribution whose centroid increases with increasing exchange time, demonstrating EX2 kinetic behavior, with a few notable exceptions (such as in the β1 strand, see below).

Unusually slow γDC hydrogen-deuterium exchange at the interface identifies a buried-interface intermediate

The V75D γDC variant populates an equilibrium intermediate in denaturant (Figure 1B), and NMR studies in 4.2 M urea revealed an unfolded NTD and a native, folded CTD (33). We carried out HDX-MS in both 4.2 M urea and 0 M denaturant (native conditions) (Figure 2A-C). In 4.2 M urea, amides in the NTD exchange quickly, within 15 seconds, while amides in the CTD are slow to exchange, with exchange rates similar to those observed under native conditions (as is expected, given the intrinsic stability of the CTD) (Figure S3). This is consistent with the structural results obtained by NMR. We term this intermediate observed under denaturing conditions the "exposed-interface intermediate."

Under native conditions (0 M denaturant), we identified a different intermediate, a conformation in which some regions of the NTD exchange too slowly to be associated with the exposed-interface intermediate. The expected stability of the exposed-interface intermediate in V75D based on our equilibrium fluorescence studies (3.5 kcal/mol, Table 1) corresponds to an average half-time for exchange of approximately 10 minutes (based on the known intrinsic exchange rates for the amides in the NTD under these conditions (51), Figure 2C). Under native conditions, almost all of the amides in NTD peptides exchange within this time frame, exhibiting complete exchange at the 60-minute timepoint (Figure 2A-C). Notably, however, amides in NTD peptides that contribute to the interface (residues 43-55 and 71-82, Figure 2D) are not completely exchanged after 60 minutes and, in fact, do not exhibit full exchange even after 96 hours (3×10^6 s), resulting in an estimated half-life of exchange $>10^4$ or 10^5 seconds. This anomalously slow exchange corresponds to a predicted ΔG value greater than 6 kcal/mol (Figure 2C), inconsistent with expectations for the exposed-interface intermediate. We therefore term the conformation associated with this new intermediate state the "buried-interface intermediate."

In order to evaluate whether this unusual behavior is unique to V75D, we monitored exchange of another variant with a destabilized NTD, the W42R variant, in which the NTD is destabilized by ~5 kcal/mol (26). Similar to V75D, the native structure of W42R exhibits no major structural changes from wild type. A minor population of a conformation with partial unfolding in the NTD was observed by solution NMR spectroscopy (26). Using HDX-MS, we find that, like V75D, W42R exhibits unexpected high protection along the interface (Figure 2E), and the exchange behavior of the exposed-interface intermediate (populated at 1.8 M GdmCl) is nearly identical to that of V75D (Figure 2A, E). Thus, W42R's HD exchange in the NTD is very similar to that of V75D (Figure S4), and both variants populate a buried-interface intermediate under native conditions.

We have no reason to expect that our data are a result of intermolecular associations, given that we have no evidence of aggregation under our experimental conditions. Moreover, NMR spectra under native conditions (concentration = 300 μM) similarly show no evidence of intermolecular associations (33).

To confirm that the unexpected slow exchange observed along the NTD interface relies on interactions with the CTD, we measured continuous hydrogen exchange behavior in the isolated γDC_{NTD} and γDC_{CTD} domains and compared these to the same regions in the full-length, wild-type γDC. All peptides in isolated domains exhibiting EX2 exchange report free energies consistent with expectations from global unfolding studies, including along the regions that comprise the interface in the full-length protein. Amides in peptides along the interface exchange faster in the isolated domains than in full-length γDC (Figure 3A, B). Because the NTD is very stable in the wild-type protein, we were unable to monitor full HD exchange in this region, and therefore no information can be obtained about the putative intermediate interface in this construct.

Changes in hydrophobic contact residues in the CTD interface destabilize the buried-interface intermediate

To probe the role of interactions from the CTD, we introduced amino acid changes into the CTD and examined the effect on the hydrogen exchange of peptides in the NTD. If interfacial

hydrophobic interactions with the CTD are contributing to the stability of the intermediate populated under native conditions (the buried-interface intermediate), then weakening these interactions, as in the V132A variant, should affect this intermediate. We carried out continuous HDX on both V132A and V75D/V132A, to measure the impact of CTD-interface variation in both wild-type and NTD-destabilized contexts.

In the V132A variant, most amides in NTD peptides (with the exception of those at the slow-exchanging interface) exchange at rates similar to, or faster than, those measured for the same region in the isolated NTD (γDC_{NTD}). While exchange in NTD interface peptides is faster for V132A than for wild-type γDC (suggesting loss of interfacial stabilization), it is still slower than in the isolated wild-type γDC_{NTD} (Figure 4A, B), indicating only partial loss of these interactions. Peptides in the CTD show similar exchange rates in both V132A and in the isolated V132A-γDC_{CTD}, except for slightly slowed exchange at the interface in the full-length protein. Exchange in the isolated V132A-γDC_{CTD} closely resembles the wild-type γDC_{CTD}, except for minor changes near position 132 (Figure S5). All together, these data suggest that the destabilization of the NTD by V132A (in the CTD) is the result of the loss of hydrophobic contacts at position 132, but that other weak interactions at the interface persist. This is consistent with our observation from the Ising analysis. In an attempt to further weaken the interface, we used the dInt-γDC variant (31, 38) and monitored its HDX behavior . Exchange rates in peptides from the NTD of dInt-γDC are mostly indistinguishable from those in the NTD of V132A γDC, suggesting that these additional changes do not weaken the interface further and only affect the intrinsic stability of the CTD (Figure S2B). This is further supported by the relative stabilities of the two unfolding transitions of dInt-γDC in denaturant (Figure S2C). Therefore, we did not study this variant further and instead focused on adding the V75D amino acid change to the V132A variant to explore the role of the interface in the newly identified intermediate accessible under native conditions.

Peptides with EX1 kinetics report on the kinetics of unfolding in the NTD
In most experiments, we observe only a few peptides whose amide exchange lies in the EX1 regime. For these peptides, the observed HDX rates report on the kinetics of the opening reaction. Peptides that exhibit this behavior reside in two locations: the first beta strand of the NTD and, under some circumstances, the NTD interface.

The first beta strand of the NTD (residues 1-7, β1) exhibits EX1 behavior in every variant investigated, including in the isolated γDC_{NTD}, indicating the presence of slow interconversion between open and closed states (Figure S6). Interestingly, neither of β1's hydrogen-bonding partners, β2 and β4, shares this EX1 behavior. The measured opening rate of the β1 strand increases upon destabilization of the NTD, whether by amino acid substitution or by addition of denaturant (Figure 5A, 5B, Table 2). When measured in V75D, the natural logarithm of this rate increases linearly with urea concentration (0.6 M - 3.0 M, m_u = 1.1 kcal mol^{-1} M^{-1} urea, Figure 5C).

To determine if this EX1 behavior is due to intrinsic local structure, we investigated the exchange behavior of a small peptide that comprises the amino acid sequence of the first 10 amino acids of γDC. Unlike in the context of the whole domain, exchange is rapid for this peptide in isolation (complete exchange < 15 s), indicating that this sequence does not exhibit any intrinsic structure. Therefore, we posit that the behavior of β1 reports on the opening kinetics of the exposed-interface intermediate. The extrapolated unfolding rate of γDC_{NTD} is ~ 0.47 s^{-1} (Figure S7) and lies within an order of magnitude of the intrinsic rate of exchange (average k_{int} for this peptide ~ 3.2 s^{-1}), justifying the assumption of EX1 kinetics.

Combining V132A with V75D (V75D/V132A) increases exchange across the entire NTD, with the most dramatic changes seen at the interface (Figure 4C, D). Under destabilizing conditions—either by adding the V132A change (V75D/V132A, Figure 4D) or the addition of urea (Figure 5B)—peptides at the domain interface show bimodal exchange. This bimodal behavior is not just a result of a switch to EX1 kinetics (as exemplified for peptide 1-7 in β1, Figure 4D), since the

centroid of the lighter peak increases with time (peptide 43-53), and instead reflects a combination of EX2 and EX1 behavior.

Interestingly, EX1 rates at the interface are equivalent to measured EX1 exchange rates in β1. The opening rate of amides at the NTD interface of V75D/V132A ($\ln(k) = -8.4 \pm 0.12$) is indistinguishable from the opening rate for β1 ($\ln(k) = -8.3 \pm 0.23$) (Figure 5A, Table 2), and in urea, opening rates at the V75D NTD interface are indistinguishable from opening rates of V75D β1 ($p = 1.0$ by one-way ANCOVA) (Figure 5C).The equivalence of EX1 exchange rates observed for amides in β1 peptides and in peptides at the NTD interface demonstrates that amides in β1 and at the interface are likely reporting on the same transition. Therefore, we conclude that the EX2 exchange at the interface is associated with the buried-interface intermediate, while, when observed, the faster-exchanging EX1 population is associated with the transition to the exposed-interface intermediate (Figure 4E, 5B).

Discussion

Many proteins associated with aggregation-related diseases have a common feature: the ability to populate a non-native or partially unfolded conformation that is more aggregation-prone than the native state (34). Characterizing these conformations and the means by which environmental and sequence factors influence this mis- or partial-folding is therefore critical to mechanistically explain these diseases. Using a combination of hydrogen-deuterium exchange/mass spectrometry and traditional chemical denaturation, we have identified and characterized intermediates on the energy landscape of γD-crystallin under both native and denaturing conditions. We find that, for two cataract-prone variants of γD-crystallin, the primary intermediate populated under native conditions is structurally and energetically distinct from the previously identified intermediate populated under chemically denaturing conditions. This new intermediate involves partial unfolding of the NTD, as compared to the full unfolding which is known to occur under mildly denaturing conditions. This newly described intermediate, the buried-interface intermediate, consists of a partially folded NTD and a fully folded CTD.

Our model for this buried-interface intermediate is based on the unexpected hydrogen exchange behavior we observe in the regions of the NTD that form the interface with the CTD. Given the thermodynamic importance of the NTD/CTD interface to NTD stability, especially in variants with an otherwise highly destabilized NTD, we expected that these interface peptides would be among the most protected regions of the NTD, but that they would either exchange at a rate consistent with the stability of the NTD unfolding transition, or else exchange in the EX1 regime if the NTD interface is slow to refold. Instead, we found that peptides along the interface in the NTD are too highly protected in EX2 for their opening transition to correspond to full unfolding of the NTD, implying the presence of an alternative intermediate population containing some degree of structure at the interface. We observe this buried-interface intermediate in both NTD-destabilized variants studied, V75D and W42R. We do not observe this anomalously slow EX2 exchange in the isolated N-terminal domain fragment γDC_{NTD}. This demonstrates that the unusually slow interface exchange only takes place in full-length γDC, and that the slow exchange behavior along the NTD interface is a consequence of interaction with the CTD, rather than being a consequence of some native misfolding or interaction taking place within the NTD itself.

The interface of γDC is crucial for the folding and stability of the NTD – particularly in NTD-destabilized variants. Our Ising analysis provides a direct measure of the strength of this interaction, and our mutational analysis demonstrates that residues at this interface are important for the formation of the buried-interface equilibrium intermediate. Moreover, we find that the population of this intermediate can be modulated by addition of denaturant or by amino acid changes at the CTD side of the interface, as seen in V132A variants. Disrupting the interface enables direct observation of both intermediates simultaneously.

Our results permit us to propose a model for V75D γDC's energy landscape (Figure 6). The buried-interface intermediate (BII) has a free energy closer to that of the native state and a lower kinetic barrier than the exposed-interface intermediate (EII). The observation of EX1 transitions in β1 and at the interface suggests two possible models: one in which BII is not on the unfolding pathway to EII (EII ⇌ N ⇌ BII, Model 1) (Figure 6A), and one in which it is (N ⇌ BII ⇌ EII, Model 2) (Figure 6B). We favor Model 1 as the most likely scenario, as outlined below.

β1 undergoes EX1 exchange under all conditions, indicating a high kinetic barrier for β1 from both BII and EII. In contrast, peptides at the interface only undergo EX1 exchange in the N → EII transition. In Model 2 (Figure 6B), there are two sequential barriers, and the closing rates of β1 for both transitions (EII → BII and BII → N) must be slow, or else EX2 exchange would be detected at β1 in one of these states. However, for interface peptides, only the EII → BII closing rate is slow, as EX2 behavior at the interface is observed in BII. This suggests that, in Model 2, EX1 exchange at interface peptides specifically reflects the BII to EII opening rate. Since EX1 exchange rates at β1 align with those at the interface, the BII to EII and N to BII opening rates are indistinguishable in this model. In Model 1 (Figure 6A), however, the two barriers (N ⇌ BII and N ⇌ EII) are not sequential, which is consistent with EX1 exchange from N → EII at both β1 and the interface. After the N → BII transition, the interface remains protected and subsequently undergoes EX2 exchange to an open state. β1 unfolds but has a slow closing rate, resulting in EX1 exchange. The relative population of each intermediate can be altered by the addition of denaturant or by amino acid substitution at the interface. This reduces the kinetic barrier to interface unfolding, permitting the simultaneous observation of both intermediates. The above reasoning implies that the buried interface intermediate is only accessed from the native state, which may have important implications for the mechanism of aggregation.

While this work cannot determine whether the identified hidden intermediate is aggregation-prone, or whether a direct link between interface stability and aggregation exists, it is highly suggestive that the buried-interface intermediate plays a role along the pathway to aggregation and cataract formation. Such equilibrium intermediates have been shown to be crucial precursors in aggregation pathways for various diseases (52). Moreover, partially folded species may be relevant conformers encountered and bound by α-crystallins (53). While *in vitro* aggregation pathways have been previously described for γDC upon rapid refolding from high concentrations of denaturant (29), such conditions are not encountered *in vivo*. In the context of aggregation from native conditions, it is important to consider excursions from the native side of the folding barrier, particularly when the kinetic barriers to unfolded states are very high.

Contrary to a simple domain-swapping model in which the entire NTD and CTD may be exchanged between monomers, the partially unfolded intermediate uncovered and characterized here retains substantial structure at the NTD-CTD interface. Some models for aggregation in γDC also include suggestions of partial unfolding of the NTD (30, 54, 55). Our data suggest that increased mobility and conformational variability across the NTD caused by a destabilizing amino acid change, combined with a local stabilizing effect of the NTD-CTD interface, results in a partially unfolded NTD, which exposes a surface that normally is buried in the full-length structure and in folded γDC_{NTD}. Thus, we suggest that it is essential to search for and describe equilibrium intermediates under experimental conditions that emulate physiological circumstances.

Materials and Methods

Detailed procedures are provided in SI Appendix.

Expression and purification of γD-crystallin variants
Mutations in the gene for wild-type γD-crystallin (from (56)) were created via site-directed mutagenesis (IDT). Mutations were confirmed by Sanger sequencing (Quintara). Wild-type and all

variant γD-crystallins except for the V75D/V132A double variant were purified as described previously (33).

Determination of stability by intrinsic tryptophan fluorescence
For each construct, two 5 μM protein stocks were prepared: a no denaturant protein stock and a high GdmCl (5.6 M) protein stock, both in PBS pH 7.0 (Sigma-Aldrich P4417), 5 mM DTT. Samples with a range of GdmCl concentrations were prepared by combination of the two stocks and allowed to equilibrate at room temperature for at least 24 hours for all constructs except wild-type, which was equilibrated for 172 hours. Measurements were then performed at 25 °C using a PTI Quantamaster Fluorometer (Horiba). An excitation wavelength of 280 nm was used to excite tryptophan residues, and emission spectra were recorded from 310 to 390 nm (0.7 s/nm). Samples were recovered from the cuvette after each measurement and the exact GdmCl concentration was determined by taking the refractive index (57). Signal was reported as a ratio of signal at 360 nm to signal at 320 nm. Signal ratios per concentration GdmCl from each variant were fit to a two-state or three-state folding model using Python's LMFIT module (58), which allowed determination of the transition midpoint, $\Delta G_{unfolding}$ and *m*-value for each transition.

To globally fit unfolding transitions of γDC variants, we generated fitting equations using a one-dimensional Ising model as described previously (44, 59). Python code modified from Marold *et. al.* (59) was used to generate and fit partition functions describing the fraction of a given folded state as a function of denaturant using separate equilibrium constants for folding of individual domains and for the interface coupling (Table S3). To fit V132A data, we modified the 1-D Ising partition function to permit coupling between the CTD and the unfolded NTD.

HDX-MS continuous exchange
Deuterated buffers were prepared by lyophilizing PBS pH 7.0 containing 5 mM DTT and resuspending in D_2O (Sigma-Aldrich 151882). All urea- and GdmCl-containing buffers were lyophilized and deuterated a total of three times to ensure total deuteration of the denaturant. Protein samples to be exchanged in the presence of denaturant were equilibrated by incubation in the requisite concentration of denaturant at 25 ˚C in PBS pH 7.0, 5 mM DTT for at least 24 hours. The peptide angiotensin-II (sequence DRVYIHPF, Thermo Scientific) was included in all samples at a concentration of 0.25 μg/mL as a fiduciary to correct for potential variability in back exchange between different buffers.

To initiate continuous labeling, samples were diluted tenfold into temperature-equilibrated, deuterated PBS buffer to produce a final γDC concentration of 7.5 μM. Samples were quenched at 15 s, 60 s, 10 min, 1 hr, 4 hr, 24 hr, and 72 hr by mixing 6 μL of the partially exchanged protein with 24 μL of quench buffer 1 (8.6 M urea, 500 mM TCEP pH 2.2) on ice. Extra time points were collected in some experiments for additional resolution. Quenching samples were incubated on ice for 1 minute to allow for partial unfolding to assist with proteolytic degradation and then were flash frozen in liquid nitrogen and stored at −80 °C. Samples were thawed by resuspension with 50 μL of ice-cold quench buffer 2 (0.75 M glycine, 50 mM TCEP, pH 2.2) to reduce denaturant concentration prior to proteolytic digestion and immediate injection onto the liquid chromatography-mass spectrometry system. Inline digestion was performed with aspergillopepsin (Sigma-Aldrich P2143) and porcine pepsin (Sigma-Aldrich P6887).

HDX-MS data analysis
Briefly, γDC peptides were identified using Byonic software (Protein Metrics) and subsequently, isotopic distributions of each peptide were fit and verified manually using HDExaminer3 (Sierra Analytics). For unimodal isotopic distributions, the monoisotopic mass for each peptide was subtracted from the mass centroid and extracted. Bimodal isotopic distributions were exported from HDExaminer3 and globally fit to a sum of two Gaussian distributions. All downstream quantitative analysis was performed using Python scripts in Jupyter notebooks.

Acknowledgments

We thank the entire Marqusee lab for experimental advice and support. This work was supported by funding from the NIH (SM), the NSF (SM), and the NEI (AMG). SM is a Chan-Zuckerberg Biohub investigator. Portions of the paper were developed from the thesis of SV.

References

1. K. W. Roskamp, C. N. Paulson, W. D. Brubaker, R. W. Martin, Function and Aggregation in Structural Eye Lens Crystallins. *Acc. Chem. Res.* **53**, 863–874 (2020).

2. H. Zhao, P. H. P. H. Brown, P. Schuck, M. T. Magone, P. Schuck, The molecular refractive function of lens γ-crystallins. **411**, 680–699 (2011).

3. H. Bloemendal, *et al.*, Ageing and vision: Structure, stability and function of lens crystallins. *Prog. Biophys. Mol. Biol.* **86** (2004).

4. S. Bassnett, On the mechanism of organelle degradation in the vertebrate lens (2009).

5. K. A. Reynolds, R. N. Mclaughlin, R. Ranganathan, Hotspots for allosteric regulation on protein surfaces https:/doi.org/10.1016/j.cell.2011.10.049 (January 29, 2019).

6. D. Pascolini, S. P. Mariotti, Global estimates of visual impairment: 2010. *Br. J. Ophthalmol.* **96** (2012).

7. J. A. Carver, J. A. Aquilina, P. G. Cooper, G. A. Williams, R. J. W. Truscott, α-Crystallin: molecular chaperone and protein surfactant. *Biochim. Biophys. Acta (BBA)/Protein Struct. Mol.* **1204** (1994).

8. J. Horwitz, α-Crystallin can function as a molecular chaperone. *Proc. Natl. Acad. Sci. USA* **89**, 10449–10453 (1992).

9. M. Delaye, A. Tardieu, Short-range order of crystallin proteins accounts for eye lens transparency. *Nature* **302**, 415–417 (1983).

10. N. E. Robinson, *et al.*, Quantitative measurement of young human eye lens crystallins by direct injection Fourier transform ion cyclotron resonance mass spectrometry. **12**, 704–711 (2006).

11. A. Basak, *et al.*, High-resolution X-ray crystal structures of human γD crystallin (1.25 Å) and the R58H mutant (1.15 Å) associated with aculeiform cataract. **328**, 1137–1147 (2003).

12. P. Evans, K. Wyatt, C. Slingsby, The P23T cataract mutation causes loss of solubility of folded γD-crystallin. *J. Mol. Biol.* **343**, 435–444 (2004).

13. Z. Xia, Z. Yang, R. Zhou, UV-radiation induced disruption of dry-cavities in human γD-crystallin results in decreased stability and faster unfolding. *Sci. Rep.* **3**, 1560 (2013).

14. S. L. Flaugh, I. A. Mills, J. King, Glutamine deamidation destabilizes human γD-crystallin and lowers the kinetic barrier to unfolding. *J. Biol. Chem.* **281** (2006).

15. E. Serebryany, *et al.*, Aggregation of Trp > Glu point mutants of human gamma-D crystallin provides a model for hereditary or UV-induced cataract. *Protein Sci.* **25**, 1115–28 (2016).

16. J. F. Hejtmancik, Congenital cataracts and their molecular genetics. *Semin. Cell Dev. Biol.* **19**, 134–149 (2008).

17. D. A. Stephan, E. Gillanders, M. J. Brownstein, Progressive juvenile-onset punctate cataracts caused by mutation of the γD-crystallin gene. *Proc. Natl. Acad. Sci. USA* **96**, 1008–1012 (1999).

18. E. Nandrot, C. Slingsby, L. Hilal, Gamma-D crystallin gene (CRYGD) mutation causes autosomal dominant congenital cerulean cataracts. *J. Med. Genet.* **40**, 262–267 (2003).

19. B. Wang, C. Yu, L. Xie, A novel CRYGD mutation (p.Trp43Arg) causing autosomal dominant congenital cataract in a Chinese family. *Hum. Mutat.* **32**, E1939–E1947 (2011).

20. E. Héon, M. Priston, F. L. Munier, The γ-crystallins and human cataracts: a puzzle made clearer. *Am. J. Hum. Genet.* **65**, 1261–1267 (1999).

21. W. Zhang, H. C. Cai, Y. B. Yan, The congenital cataract-linked G61C mutation destabilizes γD-crystallin and promotes non-native aggregation. *PLoS One* **6**, e20564 (2011).

22. J. Graw, J. Löster, M. H. de Angelis, V76D mutation in a conserved gD-crystallin region leads to dominant cataracts in mice. *Mamm. Genome* **13**, 452–455 (2002).

23. M. Roshan, P. H. Vijaya, K. Satyamoorthy, A novel human CRYGD mutation in a juvenile autosomal dominant cataract. *Mol. Vis.* **16**, 887–896 (2010).

24. W. Xu, *et al.*, A novel cataract-causing mutation Ile82Met of γA crystallin trends to aggregate with unfolding intermediate. *Int. J. Biol. Macromol.* **211** (2022).

25. K. L. Moreau, J. King, Hydrophobic core mutations associated with cataract development in mice destabilize human gammaD-crystallin. *J. Biol. Chem.* **284**, 33285–33295 (2009).

26. F. Ji, *et al.*, The human W42R γD-crystallin mutant structure provides a link between congenital and age-related cataracts. *J. Biol. Chem.* **288**, 99–109 (2013).

27. M. S. Kosinski-Collins, S. L. Flaugh, J. King, Probing folding and fluorescence quenching in human gammaD crystallin Greek key domains using triple tryptophan mutant proteins. *Protein Sci.* **13**, 2223–2235 (2004).

28. I. A. Mills, S. L. Flaugh, M. S. Kosinski-Collins, J. A. King, Folding and stability of the isolated Greek key domains of the long-lived human lens proteins γD-crystallin and γS-crystallin. *Protein Sci.* **16**, 2427–2444 (2007).

29. M. S. Kosinski-Collins, J. A. King, In vitro unfolding, refolding, and polymerization of human gammaD crystallin, a protein involved in cataract formation. *Protein Sci.* **12**, 480–490 (2003).

30. P. Das, J. A. King, R. Zhou, Aggregation of γ-crystallins associated with human cataracts via domain swapping at the C-terminal β-strands. **108**, 10514–10519 (2011).

31. S. L. Flaugh, M. S. Kosinski-Collins, J. King, Contributions of hydrophobic domain interface interactions to the folding and stability of human gammaD-crystallin. *Protein Sci.* **14**, 569–581 (2005).

32. I. A. Mills-Henry, S. L. Thol, M. S. Kosinski-Collins, E. Serebryany, J. A. King, Kinetic Stability of Long-Lived Human Lens γ-Crystallins and Their Isolated Double Greek Key Domains. *Biophys. J.* **117**, 269–280 (2019).

33. M. J. Whitley, *et al.*, A Combined NMR and SAXS Analysis of the Partially Folded Cataract-Associated V75D γD-Crystallin. *Biophys. J.* **112**, 1135–1146 (2017).

34. F. Chiti, C. M. Dobson, Protein misfolding, amyloid formation, and human disease: A summary of progress over the last decade. *Annu. Rev. Biochem.* **86** (2017).

35. S. W. Englander, T. R. Sosnick, J. J. Englander, L. Mayne, Mechanisms and uses of hydrogen exchange. *Curr. Opin. Struct. Biol.* **6** (1996).

36. A. Hvidt, K. Linderstrøm-Lang, Exchange of hydrogen atoms in insulin with deuterium atoms in aqueous solutions. *BBA - Biochim. Biophys. Acta* **14** (1954).

37. A. Hvidt, S. O. Nielsen, Hydrogen Exchange in Proteins. *Adv. Protein Chem.* **21**, 287–386 (1966).

38. S. L. Flaugh, M. S. Kosinski-Collins, J. King, Interdomain side-chain interactions in human γD crystallin influencing folding and stability. *Protein Sci.* **14**, 2030–2043 (2005).

39. K. Mandal, S. K. Bose, B. Chakrabarti, R. J. Siezen, Structure and stability of γ-crystallins. I. Spectroscopic evaluation of secondary and tertiary structure in solution. *Biochim. Biophys. Acta (BBA)/Protein Struct. Mol.* **832** (1985).

40. J. Chen, S. L. Flaugh, P. R. Callis, J. King, Mechanism of the highly efficient quenching of tryptophan fluorescence in human γD-crystallin. *Biochemistry* **45**, 11552–11563 (2006).

41. T. O. Street, N. Courtemanche, D. Barrick, Protein Folding and Stability Using Denaturants. *Methods Cell Biol.* (2008) https:/doi.org/10.1016/S0091-679X(07)84011-8.

42. D. Barrick, R. L. Baldwin, Three-State Analysis of Sperm Whale Apomyoglobin Folding. *Biochemistry* **32**, 3790–3796 (1993).

43. C. C. Mello, D. Barrick, An experimentally determined protein folding energy landscape. *Proc. Natl. Acad. Sci.* (2004) https:/doi.org/10.1073/pnas.0403386101.

44. M. Petersen, D. Barrick, Analysis of Tandem Repeat Protein Folding Using Nearest-Neighbor Models. *Annu. Rev. Biophys.* **50**, 245–265 (2021).

45. T. Kajander, A. L. Cortajarena, E. R. G. Main, S. G. J. Mochrie, L. Regan, A New Folding Paradigm for Repeat Proteins. *J. Am. Chem. Soc.* **127**, 10188–10190 (2005).

46. D. E. Makarov, A theoretical model for the mechanical unfolding of repeat proteins. *Biophys. J.* **96** (2009).

47. S. Bassnett, G. Duncan, Direct measurement of pH in the rat lens by ion-sensitive microelectrodes. *Exp. Eye Res.* **40** (1985).

48. R. Hiller, Z. H. Zhou, M. W. W. Adams, S. W. Englander, Stability and dynamics in a hyperthermophilic protein with melting temperature close to 200°C. *Proc. Natl. Acad. Sci. U. S. A.* **94** (1997).

49. D. D. Weis, T. E. Wales, J. R. Engen, M. Hotchko, L. F. Ten Eyck, Identification and Characterization of EX1 Kinetics in H/D Exchange Mass Spectrometry by Peak Width Analysis. *J. Am. Soc. Mass Spectrom.* **17**, 1498–1509 (2006).

50. Y. Bai, J. S. Milne, L. Mayne, S. W. Englander, Primary structure effects on peptide group hydrogen exchange. *Proteins Struct. Funct. Bioinforma.* **17** (1993).

51. Yu-Zhu Zhang, "Protein and peptide structure and interactions studied by hydrogen exchange and NMR," University of Pennsylvania, Philadelphia, Pennsylvania. (1995).

52. A. Horwich, Protein aggregation in disease: a role for folding intermediates forming specific multimeric interactions. *J. Clin. Invest.* **110** (2002).

53. L. Acosta-Sampson, J. King, Partially Folded Aggregation Intermediates of Human γD-, γC-, and γS-Crystallin Are Recognized and Bound by Human αB-Crystallin Chaperone. *J. Mol. Biol.* **401** (2010).

54. E. Serebryany, *et al.*, An Internal Disulfide Locks a Misfolded Aggregation-prone Intermediate in Cataract-linked Mutants of Human γD-Crystallin. *J. Biol. Chem.* **291**, 19172–19183 (2016).

55. S. Garcia-Manyes, *et al.*, Single-molecule force spectroscopy predicts a misfolded, domain-swapped conformation in human γD-crystallin protein. *J. Biol. Chem.* **291**, 4226–4235 (2016).

56. A. J. Guseman, *et al.*, Assessing the Structures and Interactions of γD-Crystallin Deamidation Variants. *Structure* **29**, 284-291.e3 (2021).

57. Y. Nozaki, the Preparation of Guanidine Hydrochloride. *Methods Enzymol.* **26** (1972).

58. M. Newville, A. Ingargiola, T. Stensitzki, D. B. Allen, Lmfit: Non-Linear Least-Square Minimization and Curve-Fitting for Python (2014) https:/doi.org/10.5281/zenodo.3712368.

59. J. D. Marold, *et al.*, A collection of programs for one-dimensional Ising analysis of linear repeat proteins with point substitutions. *Protein Sci.* **30**, 168–186 (2021).

Figures and Tables

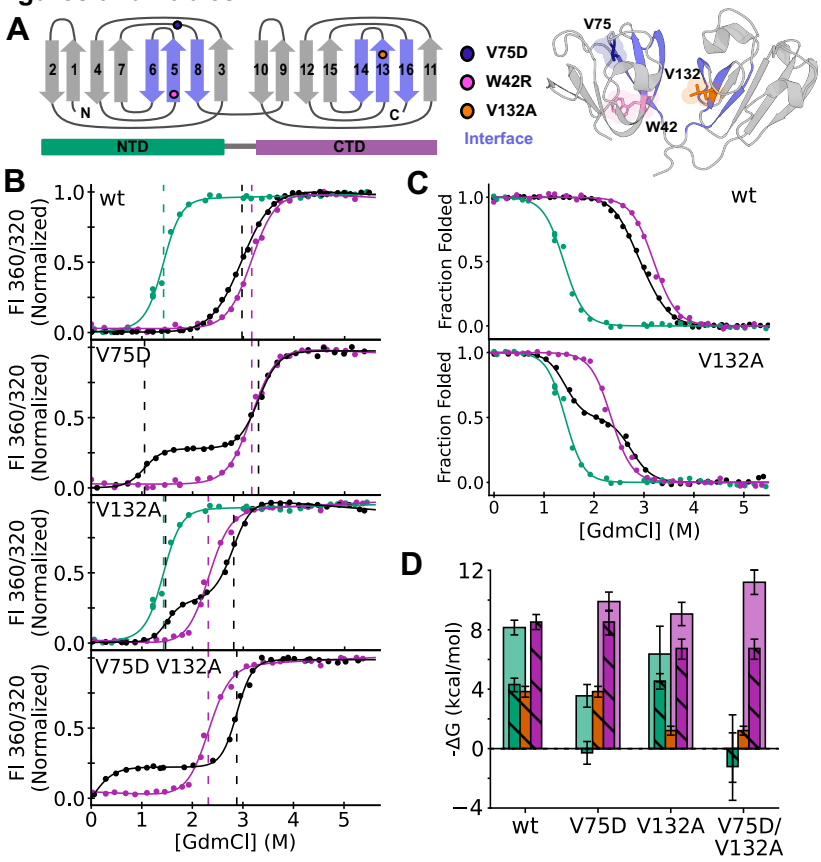

Figure 1. Equilibrium denaturation experiments of human γD-crystallin variants. A) Topological map and crystal structure (1HK0 (11)) of γDC, with Greek key beta strand architecture, NTD and CTD, and three residues of interest indicated. β-strands containing interface interactions between the two domains are highlighted in blue. B) Two- and three-state fits to tryptophan fluorescence data of full-length constructs and their corresponding isolated individual domains (γDC$_{NTD}$, green; γDC$_{CTD}$; purple; full-length γDC, black). C$_M$ values are indicated with dotted lines to draw the eye. C) Global Ising fits from analysis of the same data for V132A and wild-type (γDC$_{NTD}$, green; γDC$_{CTD}$, purple; full-length γDC, black). D) Graphical estimation of the relative energetic contributions of each domain's intrinsic stability and interfacial interaction energy to each transition (NTD, green; CTD, purple; interface, orange). Total transitions (solid bars)—that is, transitions calculated irrespective of dissection into component intrinsic and interaction energies—are taken from three-state fits, except in wild-type, where a three-state fit could not be obtained and the Ising interface and intrinsic γDC$_{NTD}$ energies were summed to estimate the total NTD transition. Intrinsic and interfacial energies (striped bars) are based on values from Ising fits. In the case of constructs containing V75D where Ising fits could not be obtained, the corresponding interaction energy in wild-type or V132A was subtracted from the construct's three-state NTD transition to estimate the intrinsic energy of V75D γDC$_{NTD}$ and V75D/V132A γDC$_{NTD}$, respectively, under the assumption that the V75D mutation does not impact the interaction energy. Error bars represent standard error of the fit. Parameters for all fits may be found in Table 2. All data were collected at 25˚C in PBS pH 7.0, 5 mM DTT.

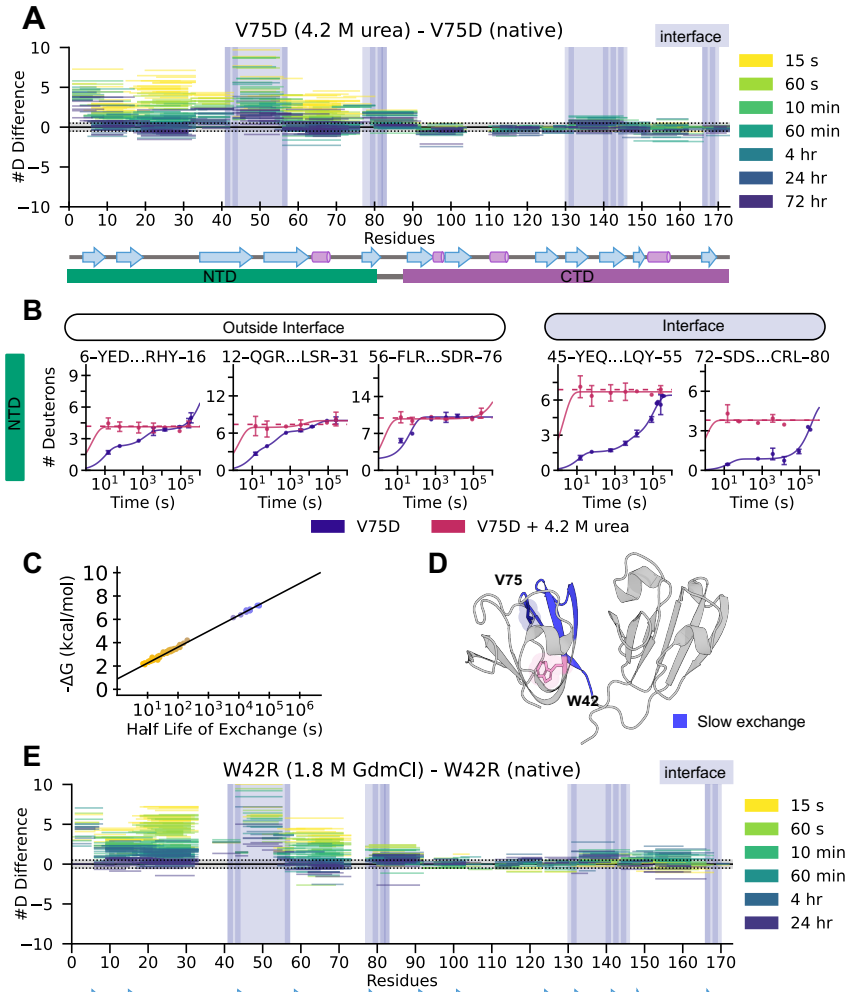

Figure 2. V75D and W42R undergo slow hydrogen-deuterium exchange at the NTD interface. A) Subtractive plot of average deuteration of V75D in urea – deuteration of V75D in native conditions for all timepoints listed. Each line represents an individual peptide spanning the residues indicated on the x-axis, with difference in number of deuterons uptaken indicated on the y-axis. A positive difference in deuteration indicates less deuteration (more protection) under native conditions than in urea. Secondary structure map and domain regions are indicated below the plot. B) Uptake plots for representative peptides in the NTD of V75D, under native conditions (blue) or in 4.2 M urea (magenta). The dotted magenta line is the average of V75D uptake in urea. The solid lines are a multiexponential fit to uptake data. Error bars represent standard deviation of technical replicates. C) Graphical illustration of the relationship between half-life of exchange and estimated ΔG for peptides in EX2. Each point is an individual peptide in the NTD of V75D, where a half-life of exchange is found by fitting uptake data to a multiexponential equation and $\Delta G_{peptide}$ is subsequently calculated based on that peptide's amide intrinsic exchange rates. The black line is the average amide intrinsic exchange rate across the entire NTD, k_{int} = 6.29 s^{-1}. Most peptides (yellow) cluster near or under the ΔG of the NTD unfolding transition of V75D, which is 3.5 ± 0.8 kcal/mol. However, some peptides (blue) exchange at a rate corresponding to a significantly higher ΔG. D) Blue regions highlighted on the crystal structure are regions of unusually slow exchange corresponding to the blue peptides in C. E) Same as A, but depicting data collected from the W42R variant either under native conditions or in 1.8 M GdmCl.

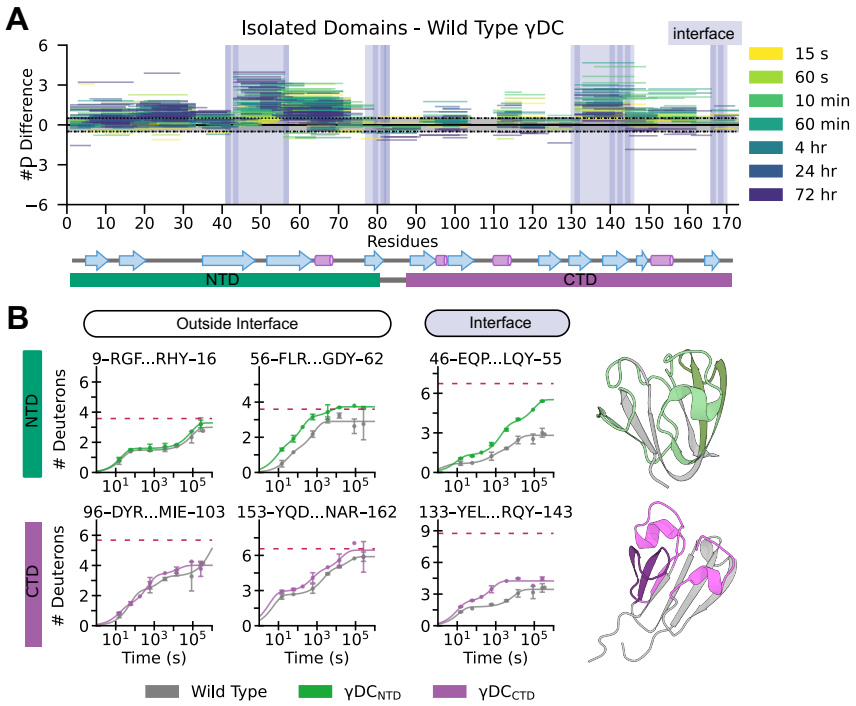

Figure 3. Isolated γDC domains lack unusual interface protection. A) Subtractive plot of deuteration of each isolated domain (γDC_{NTD} or γDC_{CTD}) – wild-type γDC. Highlighted regions on each crystal structure (γDC_{NTD}, left; γDC_{CTD}, right) indicate notable differences in deuteration. B) Representative uptake plots for comparison of wild-type and isolated domains. The dotted magenta line is average deuteron uptake for V132A in 4.2 M urea (fully exchanged comparison).

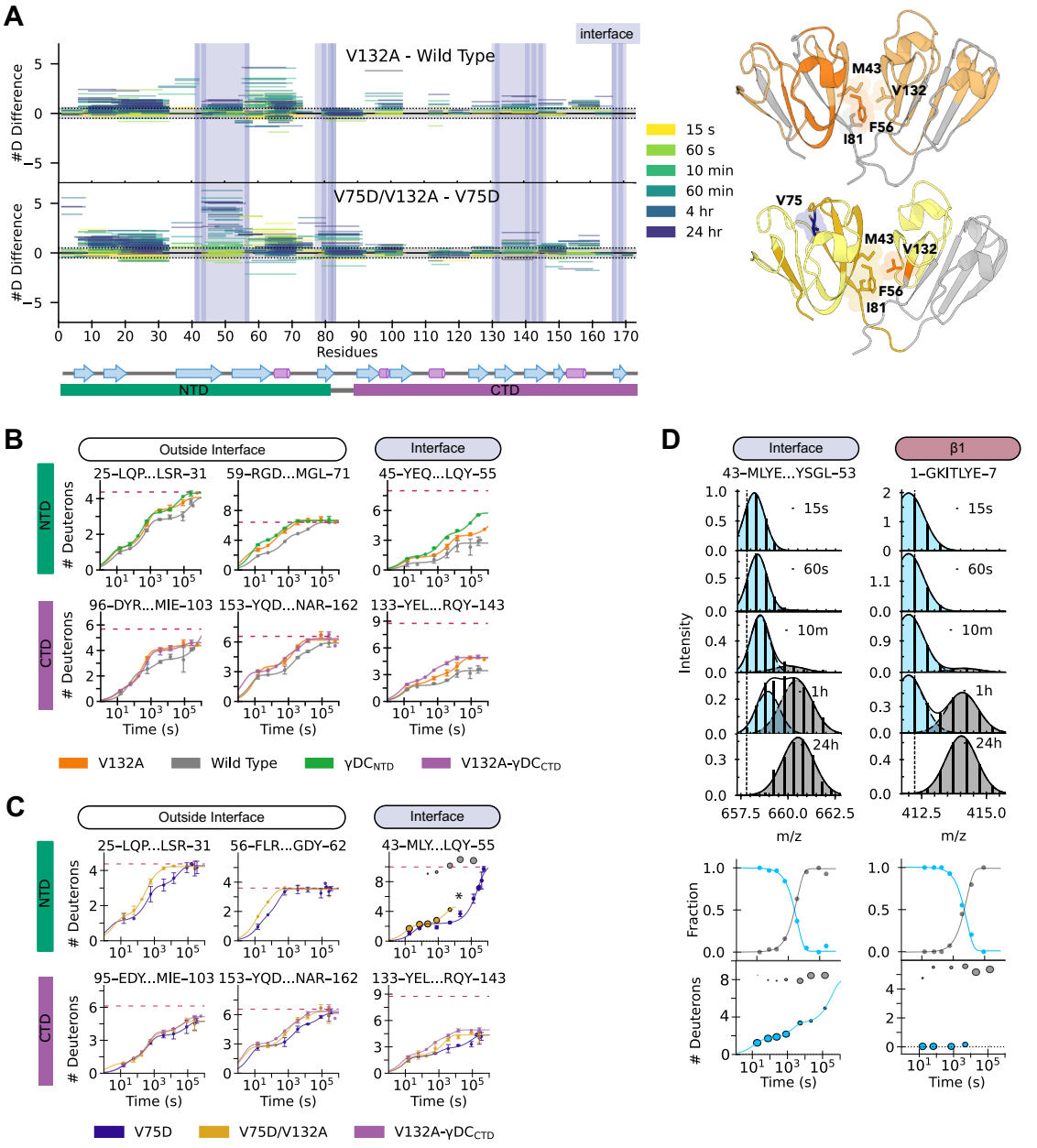

Figure 4. Disruption of the CTD interface by V132A destabilizes the native state intermediate. A) Subtractive plot of deuteration of V132A γDC – wild-type γDC (top) and V175D/V132A γDC – V75D γDC (bottom). Highlighted regions on the crystal structures indicate notable differences in deuteration (darker, more difference; gray = no difference). V132A and its three closest interacting residues in the NTD are highlighted. B) Uptake plots of V132A, wild-type γDC, and isolated domains. The dotted magenta line is average deuteron uptake of V132A in 4.8 M GdmCl (fully exchanged comparison). C) Uptake plots depicting V75D (dark blue) and V132A (yellow). The dotted magenta line is V132A in 4.8 M GdmCl (fully exchanged comparison). Peptides at the NTD interface in V75D/V132A demonstrate bimodal behavior and are plotted in yellow and gray to represent the lighter and heavier populations, respectively, where the size of the dot represents the relative population. D) Top: Representative mass spectra of two peptides in V75D/V132A as time of exchange increases, with overlaid Gaussian fits to indicate two populations (light blue, lighter, less-exchanged population; gray, heavier, more-exchanged

population). The first peptide (residues 43-53) is from the interface; the second peptide (residues 1-7) is from the β1 strand. Middle: Kinetics of conversion between the two populations, depicting change in fraction of heavy and light populations over time. Bottom: Deuteration (based on centroid mass) and relative population (depicted as the size of each dot) of the lighter (light blue) and heavier (gray) populations over time.

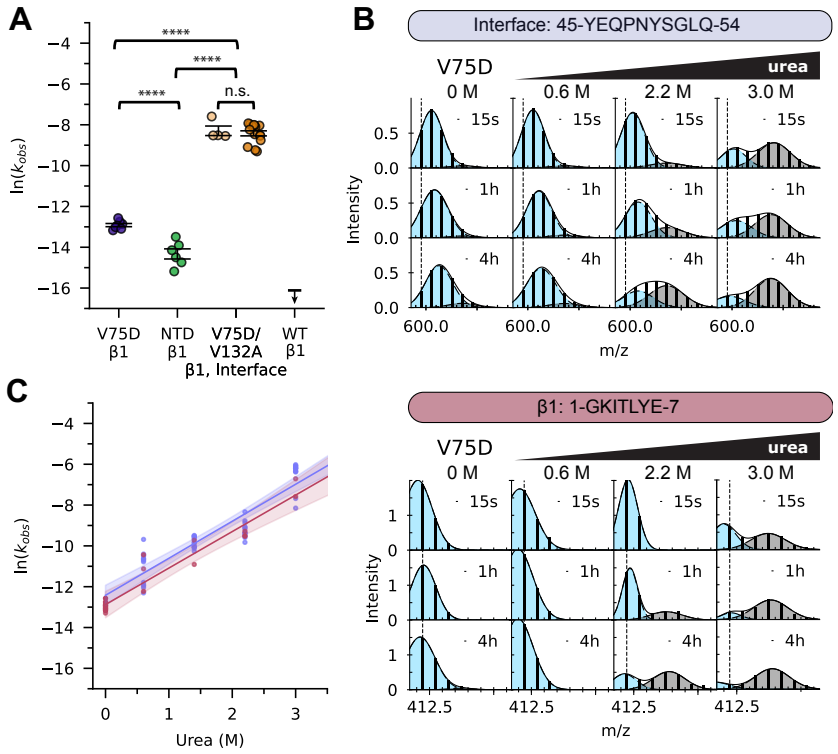

Figure 5. Rates of exchange at β1 and the buried interface correlate. A) Comparison of rates of EX1 β1 exchange in V75D (dark blue), NTD (green), and V75D/V132A (light orange), along with EX1 interface exchange in V75D/V132A (dark orange). Wild-type was too slow to measure. Error bars indicate standard error of the mean. Asterisks indicate $p < 0.0001$ by ANOVA and Tukey HSD. B) Example mass spectra of V75D peptides at the NTD interface (top) and in β1 (bottom) when equilibrated in increasing amounts of urea. C) Rates of V75D at both β1 (light red) and the NTD interface (slate blue). Shading represents 95% CI. The linear increase in EX1 opening rates of the V75D interface with respect to urea is indistinguishable from that of β1 ($p = 1.0$ by one-way ANCOVA).

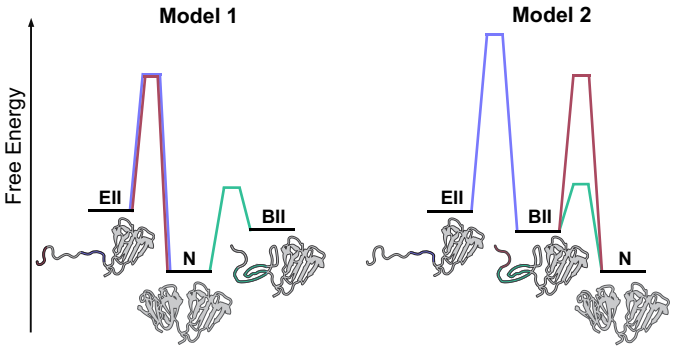

Figure 6. The energy landscape of V75D γDC. Two potential models of the energy landscape of V75D γDC, with the buried-interface intermediate either off-pathway (Model 1) or on-pathway (Model 2). Under partially denaturing conditions, NTD-destabilized γDC (V75D or W42R) populates EII. The colored kinetic barriers correspond to the observation of EX1 (large kinetic barrier) or EX2 (small kinetic barrier) exchange at the interface (slate blue), β1 (light red), or the rest of the NTD (green). In Model 1 (preferred), BII is off-pathway, whereas in Model 2, unfolding occurs through two sequential barriers which must be equivalent.

Table 1. Equilibrium two-state, three-state, and global Ising fit parameters for all γDC variants. Error reported is standard error of the fit. ΔG˚ (folding) values are in kcal/mol; C_M values are in M GdmCl; *m*-values are in kcal/(mol* M GdmCl). Confidence intervals calculated from bootstrapped parameters for Ising fits can be found in Table S1.

[(a)] The model for V132A includes a stabilizing interaction between the folded CTD and the unfolded NTD equal to that of the stabilizing interaction between the folded CTD and the folded NTD. A more complicated model permitting these two stabilizing interactions to vary independently of one another did not pass an F-test (p = 0.49) and so was not used.

		Equilibrium Transition One (NTD)			Interface	Equilibrium Transition Two (CTD)		
		ΔG°_{NTD}	**C_M**	***m*-value**	**$\Delta G^{\circ}_{interface}$**	**ΔG°_{CTD}**	**C_M**	***m*-value**
Two-State	**γDC_{NTD}**	-4.82 ± 0.53	1.43 ± 0.21	3.38 ± 0.34		--	--	--
	γDC_{CTD}	--	--	--		-7.83 ± 0.56	3.17 ± 0.33	2.47 ± 0.18
	V132A γDC_{CTD}	--	--	--		-6.21 ± 0.37	2.35 ± 0.20	2.64 ± 0.16
	Wild-type γDC	-5.86 ± 0.17	2.98 ± 0.12	1.97 ± 0.06				
Three-State	**V75D γDC**	-3.55 ± 0.76	1.05 ± 0.04	3.38 ± 0.72		-9.90 ± 0.64	3.30 ± 0.02	3.00 ± 0.19
	V132A γDC	-6.36 ± 1.87	1.47 ± 0.07	4.34 ± 1.26		-9.06 ± 0.78	2.81 ± 0.04	3.22 ± 0.27
	V132A/ V75D γDC	0.00 ± 2.27	0.00 ± 0.82	2.78 ± 2.28		-11.20 ± 0.82	2.87 ± 0.01	3.90 ± 0.29
Ising	**Wild-type γDC**	-4.47 ± 0.21	1.42 ± 0.07	3.15 ± 0.15	-3.84 ± 0.22	-8.21 ± 0.36	3.15 ± 0.06	2.61 ± 0.11
	V132A γDC	-4.53 ± 0.27	1.42 ± 0.08	3.19 ± 0.19	-1.14 ± 0.10 [(a)]	-6.66 ± 0.35	2.34 ± 0.07	2.84 ± 0.15

Table 2. Apparent EX1 HDX rates of exchange. Rates (s^{-1}) were measured at two different regions in γDC variants, the β1 strand (residues 1-7) and the interface (residues 43-55), reported as the mean of the natural log of rates (s^{-1}) obtained from distinct peptide population transitions individually fit to exponential kinetics. Error reported is standard error of the mean. Peptides were chosen from two (V75D/V132A, γDC_{NTD}) or four (V75D γDC) independent exchange experiments.

[(a)] Wild-type and V132A γDC exchanged too slowly to observe any transition in EX1 on the timescale of our experiments.

		ln(k_{op})	# peptides
β1 strand	**V75D γDC**	-12.9 ± 0.08	7
	γDC_{NTD}	-14.3 ± 0.25	6
	V75D/V132A γDC	-8.3 ± 0.23	4
	Wild-type γDC	< -16	[(a)]
	V132A γDC	< -16	[(a)]
Interface	**V75D/V132A γDC**	-8.4 ± 0.12	15